Author(s): Hinkkanen, M. & Luomi, J.

Title: Braking Scheme for Vector-Controlled Induction Motor Drives Equipped With Diode Rectifier Without Braking Resistor

Year: 2006

Version: Post print

Please cite the original version:

Hinkkanen, M. & Luomi, J. 2006. Braking Scheme for Vector-Controlled Induction Motor Drives Equipped With Diode Rectifier Without Braking Resistor. IEEE Transactions on Industry Applications. Volume 42, Issue 5. 1257-1263. ISSN 0093-9994 (printed). DOI: 10.1109/tia.2006.880852.

Braking Scheme for Vector-Controlled Induction Motor Drives Equipped With Diode Rectifier Without Braking Resistor

Marko Hinkkanen, *Member, IEEE*, and Jorma Luomi, *Member, IEEE*

***Abstract*—This paper deals with sensorless vector control of PWM-inverter-fed induction motor drives equipped with a three-phase diode rectifier. An electronically controlled braking resistor across the dc link is not used. Instead, the power regenerated during braking is dissipated in the motor while a dc-link overvoltage controller limits the braking torque. Losses in the motor are increased by an optimum flux-braking controller, maximizing either the stator voltage or the stator current depending on the speed. Below the rated speed, the braking times are comparable to those achieved using a braking resistor. The proposed braking scheme is very simple and causes no additional torque ripple. Experimental results obtained using a 2.2-kW induction motor drive show that the proposed scheme works well.**

***Index Terms*—DC-link capacitor, field weakening, flux braking, overvoltage.**

I. Introduction

Induction motor drives are usually equipped with a cost-effective diode rectifier, allowing the power flow only from the mains to the dc link. An electronically controlled braking resistor across the dc link can be used for dissipating the regenerated braking power, but it increases the price and size of a drive. An inexpensive approach is to dissipate the braking power directly in the motor. Generally, the most effective power dissipation can be achieved in low-power motors due to their large per-unit resistances.

In the conventional dc-braking method, a zero-frequency current is fed to the stator winding, resulting in zero air-gap power. DC braking is suitable only for stopping the motor, and its braking torque is small. A higher braking torque can be reached at negative slip values if the power from the stator into the inverter is controlled to zero and the motor losses are sufficient. In a method called flux braking [1], the motor losses are made higher by increasing the flux. The method is suitable for vector control, the braking can be controlled, and the motoring mode can be entered whenever desired.

An efficient but complicated braking method is proposed in [2], where a square-wave current is superimposed on the flux-producing current component. Furthermore, a PI-type dc-link overvoltage controller—limiting the braking torque based on the measured dc-link voltage—is used, but no details of the controller or its parameter selection are given. In [3], a high-frequency voltage is superimposed on the stator voltage for inducing losses but, unfortunately, large torque pulsations appear in this dual-frequency braking. A high braking torque can be achieved using high-slip braking [4], but the method is not well suited to vector-controlled drives due to the very low flux.

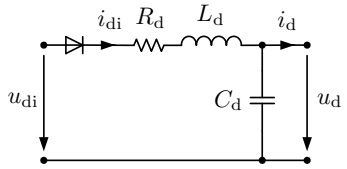

Fig. 1. Simplified model of diode rectifier and dc link.

This paper proposes a simple P-type dc-link overvoltage controller, which can be easily added to a speed or torque controller. The principle of flux braking is used to increase the losses. Depending on the speed, the proposed flux-braking controller maximizes either the stator voltage or the stator current. The losses are maximized, and the proposed controller can thus be considered as an optimum flux-braking controller. It is integrated with a field-weakening controller, resulting in fast dynamic response and smooth transitions between different operating modes.

II. System Model

A. Diode Rectifier and DC Link

The models of the drive system components are presented in the following. A simplified model of the three-phase diode rectifier and the dc link is shown in Fig. 1. The corresponding differential equations are

$$L_{\mathrm{d}}\frac{\mathrm{d}i_{\mathrm{di}}}{\mathrm{d}t} = u_{\mathrm{di}} - u_{\mathrm{d}} - R_{\mathrm{d}}i_{\mathrm{di}}, \quad i_{\mathrm{di}} \geq 0 \tag{1a}$$

$$C_{\mathrm{d}}\frac{\mathrm{d}u_{\mathrm{d}}}{\mathrm{d}t} = i_{\mathrm{di}} - i_{\mathrm{d}} \tag{1b}$$

where i_{di} is the current at the output of the rectifier and u_{di} the ideal rectified voltage. The current and the voltage at the input of the inverter are i_{d} and u_{d}, respectively. The dc-link inductance, capacitance, and resistance are L_{d}, C_{d}, and R_{d}, respectively. The mains inductance can be approximately included in the parameters L_{d} and R_{d} [5]. From (1), the rate of change of the energy stored in the capacitor can be expressed as

$$\frac{C_{\mathrm{d}}}{2}\frac{\mathrm{d}u_{\mathrm{d}}^2}{\mathrm{d}t} = u_{\mathrm{di}}i_{\mathrm{di}} - R_{\mathrm{d}}i_{\mathrm{di}}^2 - \frac{L_{\mathrm{d}}}{2}\frac{\mathrm{d}i_{\mathrm{di}}^2}{\mathrm{d}t} - p_{\mathrm{d}} \tag{2}$$

where $p_{\mathrm{d}} = u_{\mathrm{d}}i_{\mathrm{d}}$ is the power into the inverter.

B. Induction Motor and Mechanics

The dynamic model corresponding to the inverse-Γ equivalent circuit [6] of the induction motor will be used. In a general reference frame, the voltage equations are

$$\underline{u}_\mathrm{s} = R_\mathrm{s}\underline{i}_\mathrm{s} + \frac{\mathrm{d}\underline{\psi}_\mathrm{s}}{\mathrm{d}t} + \mathrm{j}\omega_\mathrm{k}\underline{\psi}_\mathrm{s} \tag{3a}$$

$$0 = R_\mathrm{R}\underline{i}_\mathrm{R} + \frac{\mathrm{d}\underline{\psi}_\mathrm{R}}{\mathrm{d}t} + \mathrm{j}\left(\omega_\mathrm{k} - \omega_\mathrm{m}\right)\underline{\psi}_\mathrm{R} \tag{3b}$$

where $\underline{u}_\mathrm{s}$ is the space vector of the stator voltage, $\underline{i}_\mathrm{s}$ the space vector of the stator current, R_s the stator resistance, and ω_k the electrical angular speed of the reference frame. The rotor resistance is R_R, the rotor current $\underline{i}_\mathrm{R}$, and the electrical angular speed of the rotor ω_m. The stator and rotor flux linkages are

$$\underline{\psi}_\mathrm{s} = \left(L'_\mathrm{s} + L_\mathrm{M}\right)\underline{i}_\mathrm{s} + L_\mathrm{M}\underline{i}_\mathrm{R}, \quad \underline{\psi}_\mathrm{R} = L_\mathrm{M}\left(\underline{i}_\mathrm{s} + \underline{i}_\mathrm{R}\right) \tag{4}$$

respectively, where L_M is the magnetizing inductance and L'_s the stator transient inductance. Iron losses are ignored here, but they will be considered in Section V.

The electromagnetic torque is given by

$$T_\mathrm{e} = \frac{3}{2}p\,\mathrm{Im}\left\{\underline{i}_\mathrm{s}\underline{\psi}^*_\mathrm{R}\right\} \tag{5}$$

where p is the number of pole pairs and the symbol * marks the complex conjugate. The equation of motion is

$$\frac{J}{p}\frac{\mathrm{d}\omega_\mathrm{m}}{\mathrm{d}t} = T_\mathrm{e} - T_\mathrm{L} - \frac{b}{p}\omega_\mathrm{m} \tag{6}$$

where J is the total moment of inertia of the mechanical system, T_L the load torque, and b the viscous friction coefficient.

The stator power can be expressed as

$$p_\mathrm{s} = \frac{3}{2}\,\mathrm{Re}\{\underline{u}_\mathrm{s}\underline{i}^*_\mathrm{s}\} = p_\mathrm{Cus} + p_\mathrm{f} + p_\mathrm{Cur} + p_\mathrm{m} \tag{7}$$

where the resistive losses in the stator and rotor are

$$p_\mathrm{Cus} = \frac{3}{2}R_\mathrm{s}i_\mathrm{s}^2, \quad p_\mathrm{Cur} = \frac{3}{2}R_\mathrm{R}i_\mathrm{R}^2 \tag{8}$$

respectively, and the rate of change of the magnetic energy is

$$p_\mathrm{f} = \frac{3}{2}\left(\frac{L'_\mathrm{s}}{2}\frac{\mathrm{d}i_\mathrm{s}^2}{\mathrm{d}t} + \frac{1}{2L_\mathrm{M}}\frac{\mathrm{d}\psi_\mathrm{R}^2}{\mathrm{d}t}\right) \tag{9}$$

The magnitude of the stator current is $i_\mathrm{s} = |\underline{i}_\mathrm{s}|$ and the magnitudes of other space vectors are defined similarly. The mechanical power is

$$p_\mathrm{m} = T_\mathrm{e}\frac{\omega_\mathrm{m}}{p} = \frac{3}{2}\frac{\psi_\mathrm{R}^2}{R_\mathrm{R}}\omega_\mathrm{r}\omega_\mathrm{m} \tag{10}$$

where $\omega_\mathrm{r} = \omega_\mathrm{s} - \omega_\mathrm{m}$ is the angular slip frequency and ω_s the angular frequency of the rotor flux. The air-gap power $p_\delta = p_\mathrm{Cur} + p_\mathrm{m}$ transferred into the rotor can be expressed as

$$p_\delta = \frac{3}{2}\frac{1}{R_\mathrm{R}}\left(\frac{\mathrm{d}\psi_\mathrm{R}}{\mathrm{d}t}\right)^2 + \frac{3}{2}\frac{\psi_\mathrm{R}^2}{R_\mathrm{R}}\omega_\mathrm{r}\omega_\mathrm{s} \tag{11}$$

The inverter is modeled by three ideal changeover switches, i.e., $p_\mathrm{s} = p_\mathrm{d}$ holds. Steady-state operation without a braking resistor is possible if the condition $T_\mathrm{L}\omega_\mathrm{m}/p + b\omega_\mathrm{m}^2/p^2 + p_\mathrm{Cus} + p_\mathrm{Cur} \geq 0$ holds.

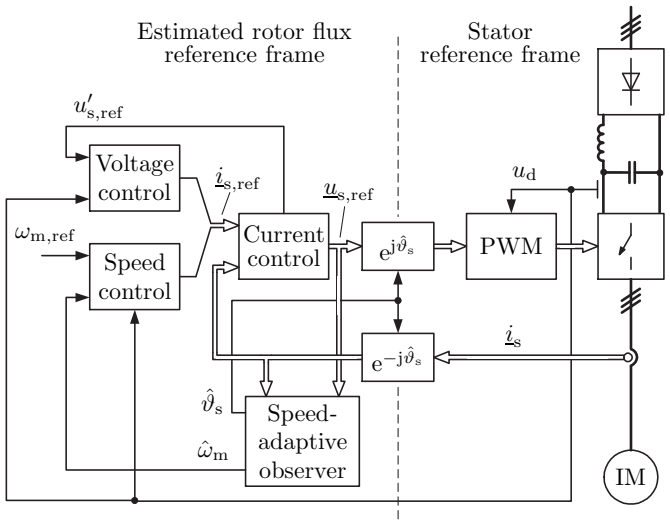

Fig. 2. Simplified block diagram of rotor-flux-oriented control system. Block "Speed control" includes speed controller augmented with proposed dc-link overvoltage controller. Block "Voltage control" includes proposed flux-braking controller integrated with field-weakening controller.

C. Speed-Sensorless Control System

In the following sections, a speed-sensorless rotor-flux-oriented control system is assumed. A simplified block diagram of the system is shown in Fig. 2. The stator current $\underline{i}_\mathrm{s}$ and the dc-link voltage u_d are measured. The rotor flux estimate (whose amplitude is denoted by $\hat{\psi}_\mathrm{R}$ and angle by $\hat{\vartheta}_\mathrm{s}$) and the rotor speed estimate $\hat{\omega}_\mathrm{m}$ can be obtained using a speed-adaptive flux observer [7], [8].

The speed controller is augmented with the proposed dc-link overvoltage controller as described in Section III. The proposed flux-braking controller is integrated with the field-weakening controller according to Section IV. This combined field-weakening and flux-braking controller is referred to as voltage controller in Fig. 2.

III. DC-Link Overvoltage Control

A. Principle

During braking, the dc-link voltage u_d rises and the current i_di decreases to zero according to (1a). When $i_\mathrm{di} = 0$, the power balance (2) reduces to

$$\frac{C_\mathrm{d}}{2}\frac{\mathrm{d}u_\mathrm{d}^2}{\mathrm{d}t} = -p_\mathrm{d} = -p_\mathrm{m} - p_\mathrm{f} - p_\mathrm{Cu} \tag{12}$$

where (7) is also used and the resistive losses are $p_\mathrm{Cu} = p_\mathrm{Cus} + p_\mathrm{Cur}$. Since the rate of change p_f of the magnetic energy is usually small compared with the other terms in (12), $p_\mathrm{f} = 0$ will be assumed. A simple proportional controller including the feedforward compensation of p_Cu can be used to control the square u_d^2 of the dc-link voltage,

$$p_\mathrm{m} = -\frac{\alpha_\mathrm{u}C_\mathrm{d}}{2}\left(u_\mathrm{d,max}^2 - u_\mathrm{d}^2\right) - \hat{p}_\mathrm{Cu} \tag{13}$$

where $u_{\mathrm{d,max}}$ is the maximum dc-link voltage and $\hat{p}_{\mathrm{Cu}}$ the estimate of the losses p_{Cu}. The feedback (13) in (12) results in the closed-loop system

$$\frac{\mathrm{d}u_{\mathrm{d}}^2}{\mathrm{d}t} = \alpha_{\mathrm{u}} \left(u_{\mathrm{d,max}}^2 - u_{\mathrm{d}}^2\right) - \frac{2}{C_{\mathrm{d}}} \left(p_{\mathrm{Cu}} - \hat{p}_{\mathrm{Cu}}\right) \tag{14}$$

where α_{u} is the bandwidth and $p_{\mathrm{Cu}} - \hat{p}_{\mathrm{Cu}}$ acts as a disturbance. According to (14), the dc-link voltage u_{d} in steady state is

$$u_{\mathrm{d}} = \sqrt{u_{\mathrm{d,max}}^2 - \frac{2}{C_{\mathrm{d}}\alpha_{\mathrm{u}}} \left(p_{\mathrm{Cu}} - \hat{p}_{\mathrm{Cu}}\right)} \tag{15}$$

B. Control Algorithm

The estimated rotor flux reference frame is considered. The components of the stator current vector correspond to $\underline{i}_{\mathrm{s}} = i_{\mathrm{sd}} + \mathrm{j}i_{\mathrm{sq}}$, and the components of other space vectors are defined similarly. Based on (10), the mechanical power p_{m} can be controlled via the electromagnetic torque or the torque-producing current component i_{sq}. The dc-link overvoltage controller can be implemented as a dynamic limit i_{squ} for the reference of the torque-producing current component,

$$i_{\mathrm{squ}} = \frac{2}{3\hat{\psi}_{\mathrm{R}}\hat{\omega}_{\mathrm{m}}} \left[\frac{\alpha_{\mathrm{u}} C_{\mathrm{d}}}{2} \left(u_{\mathrm{d,max}}^2 - u_{\mathrm{d}}^2\right) + \hat{p}_{\mathrm{Cu}}\right] \tag{16}$$

where the resistive losses can be estimated as

$$\hat{p}_{\mathrm{Cu}} = \frac{3}{2} \left[R_{\mathrm{s}}(i_{\mathrm{sd}}^2 + i_{\mathrm{sq}}^2) + R_{\mathrm{R}} i_{\mathrm{sq}}^2\right] \tag{17}$$

If the measured dc-link voltage is low-pass filtered, the bandwidth α_{u} should be substantially lower than the bandwidth of the filtering. According to (15), the bandwidth α_{u} and the capacitance C_{d} also affect the steady-state control error in u_{d} during braking.

The limits corresponding to the maximum stator current and the breakdown torque are also evaluated. The maximum stator current $i_{\mathrm{s,max}}$ is taken into account by the limit

$$i_{\mathrm{sqi}} = \sqrt{i_{\mathrm{s,max}}^2 - i_{\mathrm{sd,ref}}^2} \tag{18}$$

where $i_{\mathrm{sd,ref}}$ is the reference of the flux-producing current component. The breakdown torque is taken into account by the limit $i_{\mathrm{sqb}} = \hat{\psi}_{\mathrm{R}}/L'_{\mathrm{s}} + i_{\mathrm{sd,ref}}$, ideally corresponding to the condition $\psi_{\mathrm{sd}} = \psi_{\mathrm{sq}}$, where ψ_{sd} and ψ_{sq} are the components of the stator flux in the rotor flux reference frame.

The actual limit is the minimum of the preceding limits,

$$i_{\mathrm{sq,max}} = \begin{cases} \min\left\{i_{\mathrm{sqb}},\, i_{\mathrm{sqi}},\, i_{\mathrm{squ}}\right\}, & \text{if } i'_{\mathrm{sq,ref}}\hat{\omega}_{\mathrm{m}} < 0 \\ \min\left\{i_{\mathrm{sqb}},\, i_{\mathrm{sqi}}\right\}, & \text{if } i'_{\mathrm{sq,ref}}\hat{\omega}_{\mathrm{m}} \geq 0 \end{cases} \tag{19}$$

where $i'_{\mathrm{sq,ref}}$ is the reference of the torque-producing current component before limitation. The overvoltage limit i_{squ} is taken into account in (19) only if the estimated mechanical power is negative. The output of the speed controller is

$$i_{\mathrm{sq,ref}} = \begin{cases} i'_{\mathrm{sq,ref}}, & \text{if } |i'_{\mathrm{sq,ref}}| \leq i_{\mathrm{sq,max}} \\ \mathrm{sign}(i'_{\mathrm{sq,ref}}) i_{\mathrm{sq,max}}, & \text{if } |i'_{\mathrm{sq,ref}}| > i_{\mathrm{sq,max}} \end{cases} \tag{20}$$

Compared with the controller without the dc-link overvoltage controller, only (16) has been added and (19) modified.

IV. Flux Braking and Field Weakening

In flux braking, the motor losses are made higher by increasing the flux. The flux is limited by the maximum current at low speeds and by the maximum voltage at high speeds. For a high braking torque, the controller should thus maximize either the stator current or the stator voltage depending on the speed. In the following, the flux-braking controller is integrated with the field-weakening controller.

A. Preliminaries

Conventionally, field weakening is achieved by decreasing the flux reference inversely proportionally to the rotor speed. Alternatively, the flux reference can be determined based on the error between the reference voltage and the maximum available voltage [9]. A simpler method is obtained by excluding the conventional flux controller [10]; the flux-producing current component is controlled and limited according to[1]

$$\frac{\mathrm{d}i_{\mathrm{sd,ref}}}{\mathrm{d}t} = \gamma_{\mathrm{f}} \left[u_{\mathrm{s,max}}^2 - (u'_{\mathrm{s,ref}})^2\right], \quad -i_{\mathrm{s,max}} \leq i_{\mathrm{sd,ref}} \leq i_{\mathrm{sdN}} \tag{21}$$

where γ_{f} is the controller gain, $u_{\mathrm{s,max}}$ the maximum available stator voltage, $u'_{\mathrm{s,ref}}$ the magnitude of the unlimited voltage reference from the current controller, and i_{sdN} the rated value of the flux-producing current component. The algorithm (21) is adopted here due to its simplicity and since a flux-braking controller can easily be included in it.

The flux dynamics corresponding to the algorithm (21) can be studied using small-signal linearization. The current controller is assumed to be significantly faster than the flux dynamics. Therefore, from the viewpoint of the flux dynamics, the stator voltage components in the rotor flux reference frame are in steady state, i.e.

$$u_{\mathrm{sd}} = -\omega_{\mathrm{s}}\psi_{\mathrm{sq}} = -\omega_{\mathrm{s}} L'_{\mathrm{s}} i_{\mathrm{sq}} \tag{22a}$$

$$u_{\mathrm{sq}} = \omega_{\mathrm{s}}\psi_{\mathrm{sd}} = \omega_{\mathrm{s}} \left(\psi_{\mathrm{R}} + L'_{\mathrm{s}} i_{\mathrm{sd}}\right) \tag{22b}$$

where $R_{\mathrm{s}} = 0$ is assumed. Furthermore, $i_{\mathrm{sd,ref}} = i_{\mathrm{sd}}$ in (21) due to the fast current controller and $u'_{\mathrm{s,ref}} = u_{\mathrm{s}}$ are assumed.

The small-signal linearized model of the flux dynamics is obtained using (21) and (22), and by taking the open-loop dynamics of the rotor flux into account. The result is

$$\frac{\mathrm{d}\tilde{i}_{\mathrm{sd}}}{\mathrm{d}t} = -\frac{2\gamma_{\mathrm{f}} L'_{\mathrm{s}} u_{\mathrm{sq0}}^2}{\psi_{\mathrm{sd0}}} \left(\tilde{i}_{\mathrm{sd}} + \frac{1}{L'_{\mathrm{s}}} \tilde{\psi}_{\mathrm{R}}\right) \tag{23a}$$

$$\frac{\mathrm{d}\tilde{\psi}_{\mathrm{R}}}{\mathrm{d}t} = R_{\mathrm{R}} \tilde{i}_{\mathrm{sd}} - \frac{R_{\mathrm{R}}}{L_{\mathrm{M}}} \tilde{\psi}_{\mathrm{R}} \tag{23b}$$

where $\tilde{i}_{\mathrm{sd}}$ and $\tilde{\psi}_{\mathrm{R}}$ refer to the deviation about the operating point, and the operating-point quantities are marked by the subscript 0. The gain $\gamma_{\mathrm{f}} = R_{\mathrm{R}}\psi_{\mathrm{sd0}}/(L'_{\mathrm{s}} u_{\mathrm{sq0}})^2$ results in eigenvalues approximately at $(-1 \pm \mathrm{j})R_{\mathrm{R}}/L'_{\mathrm{s}}$, whereas a smaller γ_{f} reduces the damping. In the field-weakening operation, $\psi_{\mathrm{sd0}} \approx \psi_{\mathrm{R0}}$ and $u_{\mathrm{sq0}} \approx u_{\mathrm{dN}}/\sqrt{3}$, leading to a practical gain selection rule

$$\gamma_{\mathrm{f}} = \frac{3R_{\mathrm{R}}\hat{\psi}_{\mathrm{R}}}{(L'_{\mathrm{s}} u_{\mathrm{dN}})^2} \tag{24}$$

[1] Actually, the limitation $0.1 \cdot i_{\mathrm{sdN}} \leq i_{\mathrm{sd,ref}} \leq i_{\mathrm{sdN}}$ is used in [10].

where u_{dN} is the nominal average value of the dc-link voltage. The gain (24) equals approximately the gain proposed in [10], but is simpler to implement. According to the eigenvalues, flux dynamics fast enough can be achieved using (21), and a conventional flux controller is not needed. A detailed analysis of the algorithm (21) can be found in [10].

B. Control Algorithm

The flux-braking controller is integrated with the field-weakening controller according to

$$\frac{\mathrm{d}i_{\mathrm{sd,ref}}}{\mathrm{d}t} = \begin{cases} \gamma_{\mathrm{f}}\left[u_{\mathrm{s,max}}^2 - (u'_{\mathrm{s,ref}})^2\right], & \text{if braking or} \\ & \text{field weakening} \\ \alpha_{\mathrm{b}}\left(i_{\mathrm{sdN}} - i_{\mathrm{sd,ref}}\right), & \text{otherwise} \end{cases} \quad (25)$$

The field weakening is true if $u'_{\mathrm{s,ref}} > u_{\mathrm{s,max}}$ or $i_{\mathrm{sd,ref}} < i_{\mathrm{sdN}}$ holds. The braking is true if $i_{\mathrm{sq,max}} = i_{\mathrm{squ}}$ and $i_{\mathrm{sq,ref}} \neq i'_{\mathrm{sq,ref}}$ hold, where the limit i_{squ} is obtained from the dc-link overvoltage controller (16). Since the braking condition may change its value back and forth, a filter having the bandwidth α_{b} is used to decrease $i_{\mathrm{sd,ref}}$ to its rated value i_{sdN} after braking. The reference is limited to $-i_{\mathrm{s,max}} < i_{\mathrm{sd,ref}} < i_{\mathrm{sd,max}}$, where the maximum value is

$$i_{\mathrm{sd,max}} = \begin{cases} \sqrt{i_{\mathrm{s,max}}^2 - i_{\mathrm{squ}}^2}, & \text{if braking} \\ i_{\mathrm{s,max}}, & \text{otherwise} \end{cases} \quad (26)$$

When braking, the limit (26) allows the torque-producing current component to be controlled by the dc-link overvoltage controller, while the remaining part of the maximum current can be used to increase the losses by the flux-producing current component. The gain (24) is also used in the flux-braking mode in order to achieve smooth transitions between the flux-braking and field-weakening modes.

When braking, the maximum voltage $u_{\mathrm{s,max}} = u_{\mathrm{d}}/\sqrt{3}$ corresponding to the linear modulation region is used. Otherwise, the maximum voltage $u_{\mathrm{s,max}}$ corresponds to the inverter voltage hexagon boundaries. When the voltage reference $\underline{u}_{\mathrm{s,ref}}$ is located in the first sector, this boundary can be calculated as

$$u_{\mathrm{s,max}} = \frac{u_{\mathrm{d}}}{\sqrt{3}\sin(\vartheta + \pi/3)}, \quad 0 \leq \vartheta \leq \pi/3 \quad (27)$$

where ϑ is the angle of $\underline{u}_{\mathrm{s,ref}}$ in the stator reference frame.

V. Steady-State Characteristics

In the following, the steady-state characteristics of the proposed braking method are compared with dc braking and high-slip braking. Similar comparisons with dc braking can be found for the braking scheme based on superimposing a square-wave current on the flux-producing current component in [2, Fig. 5] and for the dual-frequency braking method in [3, Fig. 7].

The analysis is based on the motor model of Section II-B augmented with iron losses. It is assumed that the iron losses do not affect the stator current. Consequently, the power (7) in steady state can be expressed as

$$p_{\mathrm{s}} = \frac{3}{2}\left[R_{\mathrm{s}}\left(i_{\mathrm{sd}}^2 + i_{\mathrm{sq}}^2\right) + R_{\mathrm{R}} i_{\mathrm{sq}}^2 + L_{\mathrm{M}} i_{\mathrm{sd}} i_{\mathrm{sq}} \omega_{\mathrm{m}}\right] + p_{\mathrm{Fe}} \quad (28)$$

TABLE I
Data of 2.2-kW Motor Drive

Rated values of motor	
Speed	1 436 r/min
Frequency	50 Hz
Line-to-line voltage	400 V, rms
Current	5.0 A, rms
Torque T_{N}	14.6 Nm
Motor parameters	
Stator resistance R_{s}	3.7 Ω
Rotor resistance R_{R}	2.1 Ω
Stator transient inductance L'_{s}	0.021 H
Magnetizing inductance L_{M}	0.224 H
Total moment of inertia J	0.0155 kgm^2
Viscous friction coefficient b	0.0025 Nm·s
DC link	
Nominal dc-link voltage u_{dN}	540 V
Inductance L_{d}	8.1 mH
Capacitance C_{d}	235 µF

where the rotor flux reference frame is used. The stator iron losses can be approximated as

$$p_{\mathrm{Fe}} = \left[k_{\mathrm{Hy}}\frac{\omega_{\mathrm{s}}}{\omega_{\mathrm{sN}}} + (1 - k_{\mathrm{Hy}})\frac{\omega_{\mathrm{s}}^2}{\omega_{\mathrm{sN}}^2}\right]\frac{\psi_{\mathrm{s}}^2}{\psi_{\mathrm{sN}}^2} p_{\mathrm{FeN}} \quad (29)$$

The iron losses in the rated operating point are p_{FeN}, the rated angular stator frequency is ω_{sN}, and the rated stator flux ψ_{sN}. The proportion of the hysteresis losses in the rated operating point is determined by the constant k_{Hy}. In steady state, the square of the stator flux in (29) can be expressed as

$$\psi_{\mathrm{s}}^2 = \left[\left(L_{\mathrm{M}} + L'_{\mathrm{s}}\right) i_{\mathrm{sd}}\right]^2 + \left(L'_{\mathrm{s}} i_{\mathrm{sq}}\right)^2 \quad (30)$$

To avoid rising of the dc-link voltage, the stator power $p_{\mathrm{s}} \geq 0$ should hold. For loss maximization, the magnitude of the stator current should equal its maximum value, i.e., $i_{\mathrm{sd}}^2 + i_{\mathrm{sq}}^2 = i_{\mathrm{s,max}}^2$, if possible.

The steady-state characteristics of the three braking methods are evaluated assuming the rated stator current and the maximum stator voltage $u_{\mathrm{s,max}} = u_{\mathrm{dN}}/\sqrt{3}$. The data of a 2.2-kW motor given in Table I are used. The iron losses $p_{\mathrm{FeN}} = 102$ W in the rated operating point and the constant $k_{\mathrm{Hy}} = 0.75$. The magnetic saturation is taken into account by using the measured magnetizing inductance L_{M} as a function of i_{sd} [11]. The resulting braking torque and the corresponding current components as a function of the rotor speed are shown in Fig. 3.

A. DC Braking

In the dc-braking method, the angular stator frequency is $\omega_{\mathrm{s}} = 0$, leading to the air-gap power $p_\delta = 0$ in steady state according to (11), and the angular slip frequency is $\omega_{\mathrm{r}} = -\omega_{\mathrm{m}}$. The ratio of the current components in steady state is

$$\frac{i_{\mathrm{sq}}}{i_{\mathrm{sd}}} = \frac{L_{\mathrm{M}}}{R_{\mathrm{R}}}\omega_{\mathrm{r}} \quad (31)$$

The dash-dotted curves in Fig. 3 depict the achievable braking torque and the current components as a function of the rotor speed. Since the air-gap power p_δ is zero, the stator power is $p_{\mathrm{s}} = p_{\mathrm{Cus}}$ and the mechanical power is $p_{\mathrm{m}} = p_{\mathrm{Cur}} \approx (3/2) R_{\mathrm{R}} i_{\mathrm{s}}^2$.

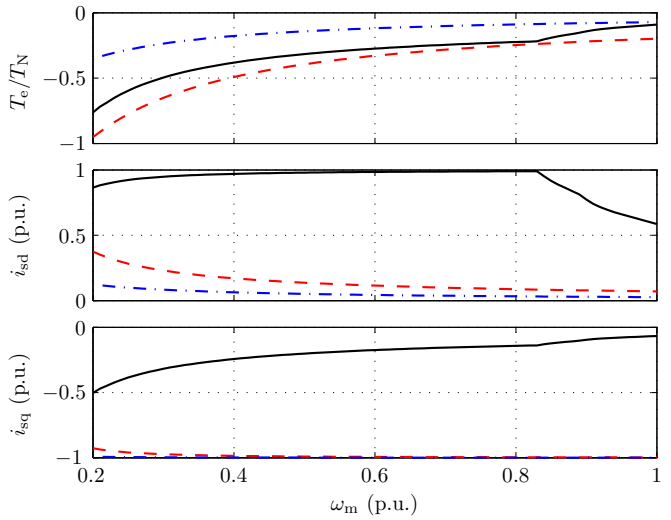

Fig. 3. Braking torque (first subplot) at rated stator current as function of rotor speed. Corresponding i_{sd} and i_{sq} are shown in second and third subplot, respectively. Solid line corresponds to proposed method, dashed line to high-slip braking [4], and dash-dotted line to dc braking. Base values are: current $\sqrt{2}$·5.0 A and angular frequency 2π·50 rad/s.

Based on Fig. 3, the rotor flux has to be decreased almost to zero. Since the rotor flux cannot be changed instantly, small values of the rotor flux are problematic if the braking is interrupted and a motoring torque is desired. Furthermore, since the slip is usually larger than the breakdown slip, the braking operation may be uncontrollable.

B. High-Slip Braking

A braking power larger than that of the dc-braking method can be achieved—without increasing the current or the maximum voltage—by controlling the stator power p_s to zero. Unlike in the dc-braking method, the stator losses also contribute to the braking power since they are fed by the motor instead of the inverter.

Inserting $p_s = 0$ into (28) and using (31), two real-valued solutions of the angular slip frequency ω_r can be obtained (except at low speeds when the losses are larger than the mechanical power). Both solutions appear in the regenerating mode, where $\omega_r\omega_s < 0$. The solution giving the larger $|\omega_r|$ corresponds to the high-slip braking method [4].

The dashed curves in Fig. 3 show the achievable braking torque and the corresponding current components as a function of the rotor speed. The mechanical power during braking is $p_m \approx p_{Cus} + p_{Cur} \approx (3/2)(R_s + R_R)i_s^2$. The braking torque is more than twice that of the dc-braking method. In both methods, the rotor flux is very small, leading to similar problems.

C. Proposed Method

The proposed method corresponds to the solution of $p_s = 0$ having the smaller $|\omega_r|$. The solid curves in Fig. 3 depict the achievable braking torque and the corresponding current components as a function of the rotor speed. It can be seen that the stator current is decreased at speeds larger than 0.83 p.u. due to the stator voltage reaching its maximum value.

The resistive stator losses p_{Cus} equal those of the high-slip braking method (at speeds lower than 0.83 p.u. in Fig. 3) while the rotor losses p_{Cur} are negligible. However, the iron losses p_{Fe} are significant since the current component i_{sd} is close to the maximum current. The mechanical power during braking is $p_m \approx p_{Cus} + p_{Fe} \approx (3/2)R_s i_s^2 + p_{Fe}$. The braking torque is larger than that of dc braking but smaller than that of high-slip braking.

The problems related to the small flux and high slip are avoided: the motoring torque can be rapidly generated and the drive can always be controlled since the slip is smaller than the breakdown slip. It is worth noticing that the proposed dc-link overvoltage controller finds $p_s = 0$ automatically by reducing $|\omega_r|$ while the proposed flux-braking controller maximizes the stator current or the stator voltage by increasing i_{sd}.

VI. Experimental Setup and Parameters

The operation of the proposed braking scheme was investigated experimentally. A 2.2-kW four-pole induction motor was fed by a frequency converter controlled by a dSPACE DS1103 PPC/DSP board, and a permanent-magnet servo motor was used as a loading machine. The data of the induction motor drive are given in Table I. The total moment of inertia J of the experimental setup is 2.2 times the inertia of the induction motor rotor.

The base values used are: current $\sqrt{2}$·5.0 A, flux 1.04 Wb, and angular frequency 2π·50 rad/s. The sampling is synchronized to the modulation, and both the switching frequency and the sampling frequency are 5 kHz. The measured dc-link voltage is filtered using a first-order low-pass filter having the bandwidth of 8 p.u. PI-type synchronous-frame current control having the bandwidth of 6 p.u. is employed [12]. The PI speed controller includes active damping [10], and its bandwidth is 0.15 p.u. The maximum stator current is $i_{s,max} = 1.5$ p.u. The bandwidth of the dc-link overvoltage controller is 0.6 p.u., the maximum dc-link voltage $u_{d,max} = 1.15 \cdot u_{dN}$, and the filter bandwidth $\alpha_b = 0.12$ p.u. in (25).

VII. Experimental Results

Fig. 4 shows experimental results of an acceleration and a speed reversal. The speed reference is stepped from zero to 1 p.u. at $t = 0.25$ s and reversed at $t = 1.25$ s. The rated load torque is applied stepwise at $t = 0.5$ s and removed at $t = 1$ s. The removal of the load torque and the speed reversal activate the braking scheme. During the braking operation, the dc-link overvoltage controller drives the power p_d to zero while the flux-braking controller increases the losses by maximizing first the stator voltage at higher speeds and then the stator current at lower speeds. It can be seen that the response in the dc-link voltage is smooth.

Operation in the field-weakening range is depicted in Fig. 5. The speed reference is stepped from zero to 3 p.u. at $t = 0.5$ s and back to zero at $t = 3$ s. Since $i_{sd,ref}$ is adjusted based on the available voltage, the current references are realizable in the field-weakening range. As predicted by the linearized model in (23), the response of the rotor flux is fast even though no conventional flux controller is used. It can be seen that the

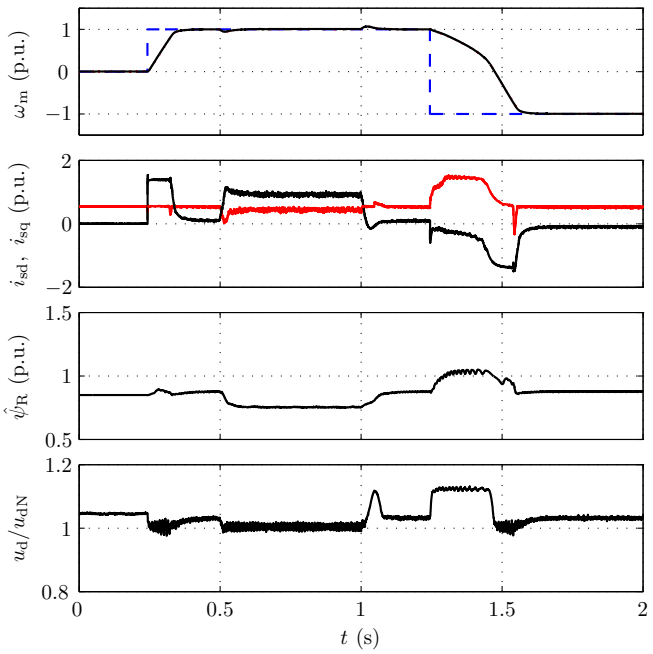

Fig. 4. Experimental results showing acceleration, load torque step, and speed reversal. First subplot shows measured speed (solid), estimated speed (dotted), and speed reference (dashed). Second subplot shows d and q components of measured stator current (solid) and their references (dashed) in estimated rotor flux reference frame. Third subplot depicts estimated rotor flux magnitude. Last subplot presents filtered dc-link voltage used in controllers.

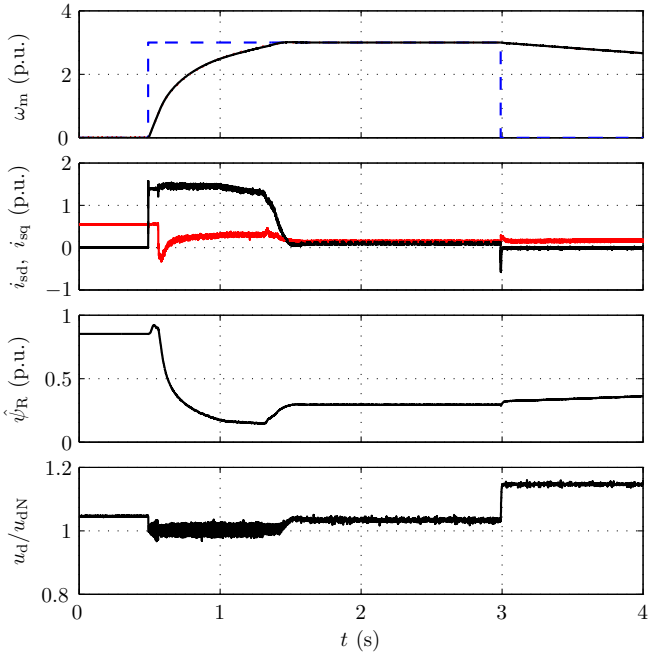

Fig. 5. Experimental results showing operation in field-weakening range. Explanations of curves are as in Fig. 4.

dc-link overvoltage controller works well and no overshoots appear in the dc-link voltage. The flux-braking principle is not useful in the field-weakening range.

Fig. 6 depicts a load torque step and its reversal at zero speed reference. The rated load torque is stepwise applied at $t = 1$ s, reversed at $t = 5$ s, and removed at $t = 9$ s. The mechanical power p_m is negative at transients, but the

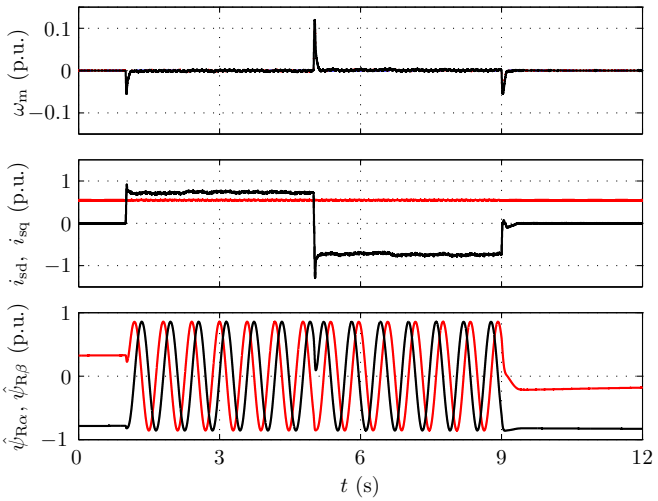

Fig. 6. Experimental results showing rated load torque step and its reversal at zero speed reference. First subplot shows measured speed (solid), estimated speed (dotted), and speed reference (dashed). Second subplot shows d and q components of measured stator current (solid) and their references (dashed) in estimated rotor flux reference frame. Last subplot depicts components of estimated rotor flux in stator reference frame.

losses are larger than $|p_m|$. The limit i_{squ} in (16) is large at low speeds, and the torque is thus not limited by the dc-link overvoltage controller. Depending on the values of the capacitance C_d, the bandwidth α_u, and the maximum dc-link voltage $u_{d,max}$, the limit i_{squ} may become too small at low speeds unless the feedforward compensation $\hat{p}_{Cu}$ is used. The accuracy of $\hat{p}_{Cu}$ is not crucial, however.

VIII. Conclusion

In the proposed braking scheme, the braking power is effectively dissipated in the motor and, consequently, an electronically controlled braking resistor is avoided. The losses in the motor are increased by an optimum flux-braking controller, maximizing either the stator voltage or the stator current, depending on the speed. Experimental results show that the proposed scheme works well. The dc-link overvoltage controller regulates the dc-link voltage without overshoots. The braking scheme is very simple, allows significant reduction of the braking time below the rated speed, and causes no additional torque ripple.

Acknowledgment

The authors gratefully acknowledge the financial support given by ABB Oy.

References

[1] P. Tiitinen and M. Surandra, "The next generation motor control method, DTC direct torque control," in *Proc. IEEE PEDES'96*, vol. 1, New Delhi, India, Jan. 1996, pp. 37–43.

[2] J. Jiang and J. Holtz, "An efficient braking method for controlled ac drives with a diode rectifier front end," *IEEE Trans. Ind. Applicat.*, vol. 37, no. 5, pp. 1299–1307, Sept./Oct. 2001.

[3] M. Rastogi and P. W. Hammond, "Dual-frequency braking in AC drives," *IEEE Trans. Power Electron.*, vol. 17, no. 6, pp. 1032–1040, Nov. 2002.

[4] M. M. Swamy, T. Kume, Y. Yukihira, S. Fujii, and M. Sawamura, "A novel stopping method for induction motors operating from variable frequency drives," *IEEE Trans. Power Electron.*, vol. 19, no. 4, pp. 1100–1107, July 2004.

[5] P. C. Krause, O. Wasynczuk, and S. D. Sudhoff, *Analysis of Electric Machinery and Drive Systems*. Piscataway, NJ: IEEE Press, 2002.
[6] G. R. Slemon, "Modelling of induction machines for electric drives," *IEEE Trans. Ind. Applicat.*, vol. 25, no. 6, pp. 1126–1131, Nov./Dec. 1989.
[7] M. Hinkkanen, "Analysis and design of full-order flux observers for sensorless induction motors," *IEEE Trans. Ind. Electron.*, vol. 51, no. 5, pp. 1033–1040, Oct. 2004.
[8] M. Hinkkanen and J. Luomi, "Stabilization of regenerating-mode operation in sensorless induction motor drives by full-order flux observer design," *IEEE Trans. Ind. Electron.*, vol. 51, no. 6, pp. 1318–1328, Dec. 2004.
[9] H. Grotstollen and J. Wiesing, "Torque capability and control of a saturated induction motor over a wide range of flux weakening," *IEEE Trans. Ind. Electron.*, vol. 42, no. 4, pp. 374–381, Aug. 1995.
[10] L. Harnefors, K. Pietiläinen, and L. Gertmar, "Torque-maximizing field-weakening control: design, analysis, and parameter selection," *IEEE Trans. Ind. Electron.*, vol. 48, no. 1, pp. 161–168, Feb. 2001.
[11] M. Hinkkanen and J. Luomi, "Parameter sensitivity of full-order flux observers for induction motors," *IEEE Trans. Ind. Applicat.*, vol. 39, no. 4, pp. 1127–1135, July/Aug. 2003.
[12] F. Briz, M. W. Degner, and R. D. Lorenz, "Analysis and design of current regulators using complex vectors," *IEEE Trans. Ind. Applicat.*, vol. 36, no. 3, pp. 817–825, May/June 2000.

Marko Hinkkanen (M'06) was born in Rautjärvi, Finland, in 1975. He received the M.Sc.(Eng.) and D.Sc.(Tech.) degrees from Helsinki University of Technology, Espoo, Finland, in 2000 and 2004, respectively.

Since 2000, he has been a Research Scientist with the Power Electronics Laboratory, Helsinki University of Technology. His main research interest is the control of electric drives.

Jorma Luomi (M'92) received the M.Sc.(Eng.) and D.Sc.(Tech.) degrees from Helsinki University of Technology, Espoo, Finland, in 1977 and 1984, respectively.

In 1980, he joined Helsinki University of Technology, and from 1991 to 1998, he was a Professor at Chalmers University of Technology. Since 1998, he has been a Professor with the Department of Electrical and Communications Engineering, Helsinki University of Technology. His research interests are in the areas of electric drives, electric machines, and numerical analysis of electromagnetic fields.